Competing magnetic structures and magnetic transitions in Er_2Ni_2Pb: Powder neutron diffraction measurements

K. Prokeš
Helmholtz-Centre Berlin for Materials and Energy, SF-2, Glienicker Straβe 100, Berlin 14109, Germany

E. Muñoz-Sandoval
Advanced Materials Department, IPICyT, Apartado Postal 3-74, Tangamanga, San Luis Potosi 78231 Mexico

Aravind D. Chinchure
Materials Research Laboratory, John F. Welch Technology Center, Bangalore 560 066, India

J. A. Mydosh
Institute of Physics II, University of Cologne, Cologne 50937, Germany
and Kammerlingh Onnes Laboratory, Leiden University, 2300 RA Leiden, The Netherlands
(Received 7 March 2008; revised manuscript received 13 May 2008; published 23 July 2008)

We have studied the magnetic structures of Er_2Ni_2Pb using a powder neutron diffraction technique in zero field. Previous bulk measurements suggested three distinct magnetic phase transitions. Our neutron diffraction experiments, which were made in the range 1.5−5 K, showed that magnetic Bragg reflections in Er_2Ni_2Pb can be indexed by several propagation vectors that coexist over an extensive temperature range. Rather than a homogeneous magnetic structure that is simultaneously described by all the existing propagation vectors, several spatially separated structures appear to exist in Er_2Ni_2Pb. The appearance/disappearance of representative reflections at $T_N=3.5$ K, $T_{m1}=3.0$ K, $T_{m2}=2.3$ K, and $T_{m3}=1.8$ K denote magnetic phase transitions. The only magnetic state that is determined by a single propagation vector exists just below T_N. In all other magnetic states, more than one propagation vectors are stable. Except for the lowest temperature state, which is commensurate, all other propagation vectors are incommensurate with respect to the crystal structure. Although the coexistence of several spatially separated magnetic structures can be explained by the competition of magnetic interactions along particular crystallographic directions, some of the details, e.g., the exact ground-state magnetic structure, are still unclear and need further study.

DOI: 10.1103/PhysRevB.78.014425 PACS number(s): 75.25.+z, 61.05.fm

I. INTRODUCTION

Magnetic materials with unconventional properties are of particular interest and importance in both fundamental and applied research.[1] A few years ago, a large family of R_2T_2X intermetallic compounds that exhibit rather interesting magnetic properties was synthesized and studied by various groups.[2–10] Rare-earth elements Y, Nd, and from Gd to Lu can be combined with T=Ni and X=Pb. Detailed bulk measurements suggest that the only magnetic element in these materials is the rare-earth ion. Ni and Pb do not carry any magnetic moment. The crystal structure has orthorhombic symmetry of the Mn_2AlB_2 type and the space-group *Cmmm* in the literature.[2] This structure type is also denoted as the AlB_2Fe_2.[11] All the R atoms are equivalent. They occupy the same crystallographic position, building two zigzag chains running along the a axis. Due to the nonmagnetic elements surrounding the R atoms, a significant magnetocrystalline anisotropy exists, and such an anisotropy can lead to an unusual or multiple magnetic phase transitions and/or complex magnetic-moment arrangements. Indeed, it was previously found from single-crystal and neutron powder experiments on Dy_2Ni_2Pb (Ref. 5) and Ho_2Ni_2Pb (Ref. 10) that magnetic structures in these compounds are unusually complex, and consequently very challenging. However, not all their details are understood. Especially, one particular question has not been answered, namely, why the two chains of similar magnetic atoms are different.

From combined measurements of magnetic susceptibility, magnetization specific heat, electrical resistivity, and magnetoresistance on polycrystalline and/or single-crystalline samples of Er_2Ni_2Pb,[4,6] it has been suggested that three different and complex, most probably antiferromagnetic (AF) or ferromagnetic (F) phases appear at low temperature. Three magnetic phase transitions at $T_{N1}=3.4$ K, $T_{N2}=3.2$ K, and $T_{N3}=2.0$ K were observed.[6] In contrast, Gulay *et al.*[3] reported for Er_2Ni_2Pb a ferromagnetic phase transition taking place at $T_C=6.0$ K with additional antiferromagnetic phase transition appearing around 3.5 K. Similar discrepancy in the type of the magnetic ordering was found also for Ho containing system.[3,10] We believe that such an unsatisfactory situation of contradictory magnetic states and phase-transition temperatures requires clarification.

A common feature of all the magnetic phases in all the R_2Ni_2Pb compounds is their sensitivity to applied magnetic field and strong magnetocrystalline anisotropy. Sharp metamagnetic-like transitions and a giant magnetoresistance accompanying these transitions were observed also in Er_2Ni_2Pb. Two transitions in fields below 2 T were identified for fields applied along the a and the b axes, leading to saturated magnetization of 6 and $8\mu_B$/Er above 3 T for field along the a and the b axis, respectively. Electrical resistivity

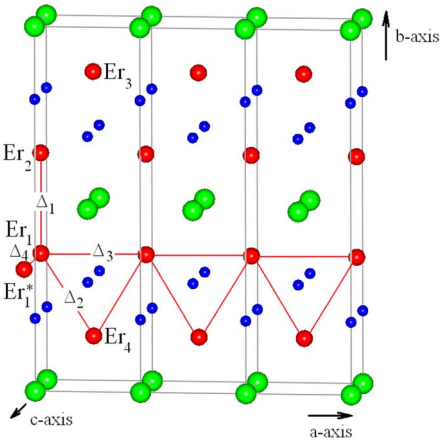

FIG. 1. (Color online) Orthorhombic crystal structure (*Cmmm*) of R_2Ni_2Pb compounds (R stands for Gd to Lu, Y, and Sm). The unit cell is indicated by the dark lines. The largest, medium, and smallest spheres represent Pb, R, and Ni atoms, respectively. The labeling of atoms Er_1 at 0, 0. 3603, $\frac{1}{2}$, Er_2 at 0, 0.6397, $\frac{1}{2}$, Er_3 at $\frac{1}{2}$, 0.8603, $\frac{1}{2}$, and Er_4 at $\frac{1}{2}$, 0.1397, $\frac{1}{2}$ is used to describe the magnetic structure. The shortest distances along particular directions, as discussed in the text, are indicated.

reductions of 12(13)% for the *a* (*b*) axis have been observed at the transition.[4,6] The *c* axis is, in Er_2Ni_2Pb, the hard magnetization axis with no metamagneticlike transition below 10 T. In order to identify the relation between macroscopic bulk magnetic properties and microscopic arrangements of Er moments, and to clarify whether the magnetic state is ferromagnetic or antiferromagnetic (actually, the magnetization studies[4] suggest quite strongly that the ground state is antiferromagnetic), we have investigated this material by means of a neutron diffraction at low temperatures.

II. EXPERIMENT

Er_2Ni_2Pb possesses an unusually anisotropic orthorhombic crystal structure with the space-group *Cmmm* (Fig. 1).[2] The *b* axis is about four times longer than the other two principal axes leading to very different growth rates. As a consequence, one can extract from polycrystalline bulk pieces relatively large single-crystal grains but, at the same time, one has problems with the preferential orientation in powder experiments. Planes consisting only of *R* are intercalated between planes of only Pb atom on one side and Ni atoms on the other. These are stacked along the *b* axis in the sequence Pb-Er-Ni-Er-Pb-Er-Ni-Er-Pb.

The sample was prepared by arc melting pure elements on a water-cooled copper hearth under purified Ar atmosphere. After flipping and remelting the ingots a few times in order to achieve good homogeneity, the sample was heat treated for 4 weeks at 870 K in an evacuated quartz ampoule. Finally, determination of the stoichiometry and homogeneity using electron probe microanalysis (EPMA) was conducted. The sample was found to be single phase with the desired 2:2:1 stoichiometry of ± 2 at. %.

Neutron diffraction patterns were collected at selected temperatures between 1.5 and 8.5 K using the multicounter diffractometer E9 installed at the Berliner Neutron Scattering Center (BENSC) at the Hahn-Meitner-Institute. The E9 diffractometer is equipped with a detector bank that covers 160°. However, it consists of individual ^{3}He tubes, each able to detect neutrons only at a particular place within a range of 2.5° with a resolution of about 10 min. Therefore, in order to obtain the whole pattern, it is necessary to perform 25–32 steps within the given range of 2.5°. The incident-neutron wavelength was 1.7988 Å and an ILL orange-type cryostat has been employed to achieve low temperatures. For these measurements about 7 g of Er_2Ni_2Pb was ground under inert atmosphere and encapsulated into a vanadium container with He gas. The data were collected for 8 h at each of the four selected temperatures that were chosen in order to have representative set of data for each magnetic state. The data were analyzed by means of the Rietveld profile procedure[12] using the computer code FULLPROF, which is a part of a larger package WINPLOTR.[13] The Er magnetic form factor was taken from Ref. 14. To trace magnetic phase transitions, we have also followed the temperature development of peak intensities by measuring patterns at 27 different temperatures with a step of about 0.1 K for about 1 h each.

III. NEUTRON DIFFRACTION RESULTS

A. Paramagnetic state

Inspection of the powder neutron diffraction pattern recorded at 4.45 K in the paramagnetic state of our Er_2Ni_2Pb revealed systematic extinction of reflections, which is in accord with the space-group *Cmmm*. Further refinements confirm that this compound crystallizes in the orthorhombic Mn_2AlB_2 type of structure reported for this compound in the literature.[2] Diffraction data were corrected for absorption. Results of the best fit comprising the scale factor, lattice cell parameters, crystallographic-position parameters, isotropic thermal factor for each atom, and background and peak-profile parameters at 4.45 K are summarized in Table I. The fit itself, with the experimental data, is shown in Fig. 2. Inclusion of the occupation parameters to the fit as free parameters did improve its quality by few percents. Although our sample has stoichiometry close to the ideal 2:2:1 ratio, 2% and 6% deficiencies of Ni and Pb were detected, respectively. Due to the highly anisotropic shape of the crystallographic unit cell, we had to also include a preferential orientation parameter. Let us note that no ferromagnetic signal has been detected.

All the Er atoms in the unit cell occupy the 4*j* position at 0, y_{Er}, $\frac{1}{2}$ with the local symmetry *m*2*m*, and are crystallographically equivalent. Ni atoms occupy 4*i* positions at 0, y_{Ni}, 0, and Pb atoms occupy the 2*a* Wyckoff position 0, 0, 0. There are four Er atoms in the crystallographic unit cell. We denote these atoms as Er_1 at 0, 0.3603, $\frac{1}{2}$, Er_2 at 0, 0.6397, $\frac{1}{2}$, Er_3 at $\frac{1}{2}$, 0.8603, $\frac{1}{2}$, and Er_4 at $\frac{1}{2}$, 0.1397, $\frac{1}{2}$. The symmetry operations include a $(\frac{1}{2}, \frac{1}{2}, 0)$ translation. This, together with the fact that some of the Wyckoff positions are (apart from translation) symmetry equivalent, leads to different values for the atomic positions in the literature. An interesting point is that the Er atoms form two chains, each consisting of a

TABLE I. Structural parameters of Er_2Ni_2Pb determined above the magnetic phase transition (in the paramagnetic state) at 4.5 K using powder neutron diffraction.

Space group		*Cmmm*		
Para, T=4.45 K				
Atom	Site	Pos. Param.	B (Å)	Occupation
Er	4*j*	0, 0.3603 (3), $\frac{1}{2}$	0.22 (5)	1.00 (fixed)
Ni	4*i*	0, 0.2000 (3), 0	0.18 (8)	0.986 (2)
Pb	2*a*	0, 0, 0	0.20 (3)	0.961 (3)
Lattice constants (Å)		a=4.0021(1)	b=13.8984(6)	c=3.6111(1)
Agreement factors:		R_p=6.90%	R_B=9.01%	

nearly triangular net. The distance, Δ_1, between the atom Er_1 and the atom Er_2 is equal to, according to our refinement, 3.883 Å. The distance between the Er_1 and Er_4 (along the *b* axis), Δ_2, amounts to 3.6612 Å, and that between the Er_1 and next Er_1 atom in the next crystal cell along the *a* axis is Δ_3=4.004 Å, equal to the *a* axis lattice constant. The distance between the Er moments along the *c* axis, Δ_4=*c* axis constant (3.61 Å). The largest relative difference between the Er distances within the *a*-*b* plane is 9%. This value is somewhat larger than in the case of Dy_2Ni_2Pb.[5] This suggests that there might be a larger magnetic anisotropy in the Er containing system because of anisotropic RKKY interactions that are mediated by Ni atoms, which occupy the 4*i* positions at 0, y_{Ni}, 0, and by Pb atoms in the 2*a* Wyckoff position 0,0,0.

B. Temperature dependence of Bragg reflections

As the temperature is lowered, new Bragg reflections appear. These reflections are assumed to be due to magnetic order. In Fig. 3 we show an interpolated contour intensity plot resulting from 27 short-time scans. The integrated intensities are shown in Fig. 4. We note that all the low-angle reflections are resolution limited. Two of the reflections, B=(020) and J=(110) that exist already at higher temperatures, are of nuclear origin. However, while the B=(020) reflection has, within the error bars, a constant integrated intensity across the whole temperature range, the J=(110) reflection shows appreciable temperature dependence that will be discussed later. The paramagnetic-antiferromagnetic phase transition is clearly indicated by the appearance of reflections C and I at T_N=3.5 K, whose positions are not indexable with integer indices. Obviously, the magnetic order is at least partly antiferromagnetic in nature below this temperature. With further lowering the temperature below T_{m1}=3.0 K, two new reflections, namely F and G, appear. While the F reflection exists down to 1.5 K, the reflections C, G, and I disappear around T_{m2}=2.2 K, i.e., around the same temperature where two other reflections, E and H appear, and where also reflection J substantially increase in

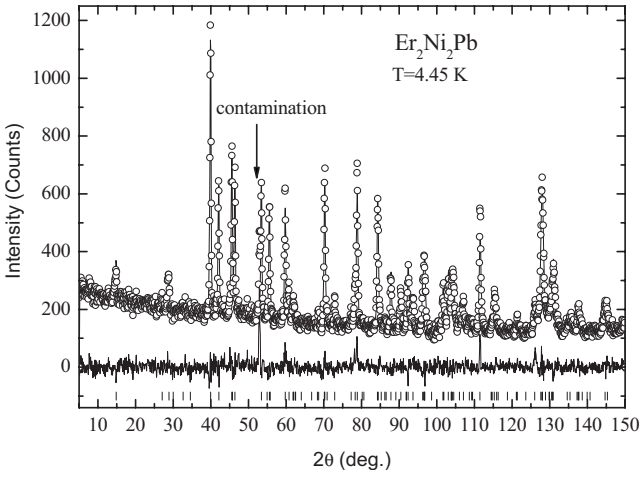

FIG. 2. The diffraction data (circles) of Er_2Ni_2Pb were taken in the paramagnetic state at 4.45 K together with the best fit (the full line through points) and the difference between them (line at the bottom). Crystal structure Bragg reflection positions are tick marked at the bottom. Contamination due to sample environment is denoted by an arrow. For numerical results, see Table I.

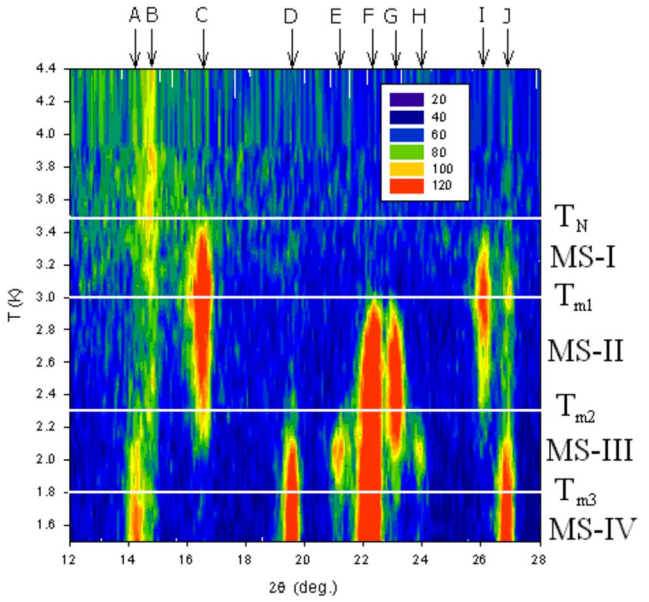

FIG. 3. (Color online) Contour intensity plot showing the low angle portion of diffraction patterns taken on Er_2Ni_2Pb versus temperature. The ten Bragg reflections denoted by arrows are described in the text. The various phases, as discussed in the text, are labeled and their relevant ordering temperatures are indicated on the right-hand side.

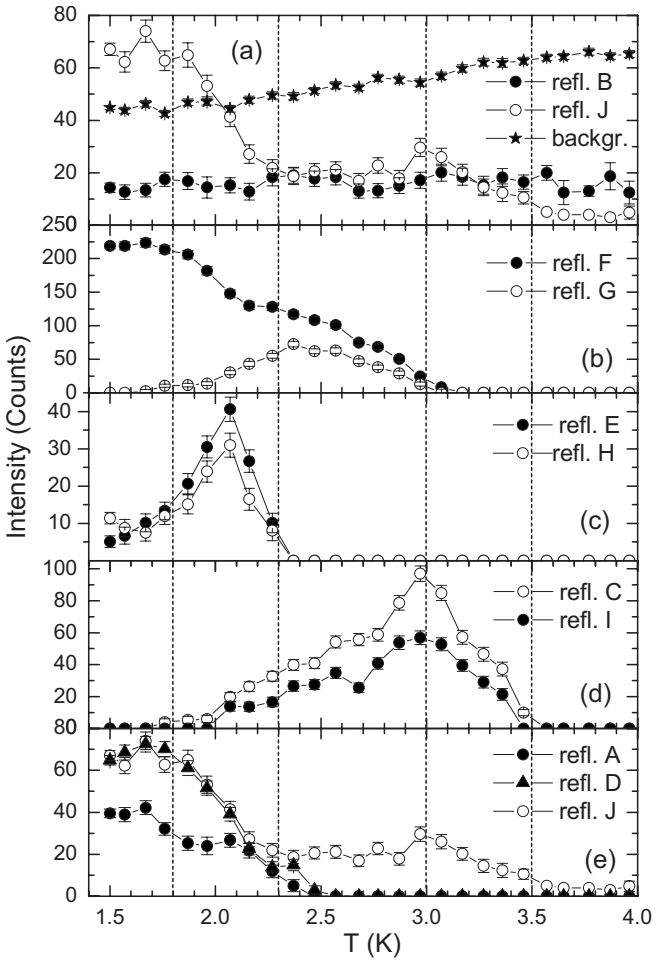

FIG. 4. Temperature dependence of integrated intensities of the ten lowest positioned reflections (denoted by A–J) of Er_2Ni_2Pb, determined from fitting of data shown in Fig. 3. The identification of individual reflections is given in the text. The dashed lines represent the suggested magnetic phase transitions.

intensity. While the *E* and *H* reflections attain the maximum intensity around 2.0 K and nearly vanish below $T_{m3}=1.8$ K, the *A*, *D*, *F*, and *J* reflections gain in intensity down to 1.5 K, the lowest temperature of the experiment. The latter two exhibit a two-step increase. We assume that at the positions of the *F* and *J*, different Bragg reflections contribute. In contrast, the *E* and *H* reflections almost disappear in the low-*T* limit. An interesting observation is that here an extensive temperature overlap exists (e.g., reflections *C* and *G*) and that one group of reflections exhibits a maximum at the temperature where another group appears (reflections *E* and *H* versus *F* and *G*) or disappears (*C* and *I* versus *F* and *G*). This suggests either that some magnetic phases coexist or that, at certain temperatures, the magnetic phases are described by more than one propagation vector. We denote the magnetic state between the $T_N=3.5$ K and $T_{m1}=3.0$ K as magnetic state I (MS-I), between T_{m1} and $T_{m2}=2.3$ K as MS-II, between T_{m2} and $T_{m3}=1.8$ K as MS-III, and below T_{m3} as MS-IV.

Let us consider at first the MS-I state, then we deal with the MS-IV state, and finally, we describe the analysis of the two most complicated states, MS-II and MS-III.

C. MS-I state between the $T_N=3.5$ K and $T_{m1}=3.0$ K

Characteristic for the phase MS-I is the existence of reflections *C* and *I*. It appeared that these reflections can be indexed by a propagation vector of the form $q_I=(k_x,0,\frac{1}{2})$ with $k_x\approx 0.16$ or 0.84. This suggests a doubling along the *c* axis and a sine-wave modulation along the *a* axis. With the $k_x\approx 0.84$, one can index the *C* and the *I* reflections in Figs. 3 and 4 as being composed of $(1-11)^-$, $(110)^-$, $(1-10)^-$, and $(111)^-$ for the former (*C*), and $(000)^{+-}$ and $(001)^-$ for the latter (*I*) one, respectively. At the same time one can identify that the increase of the *J* reflection [see Fig. 4(e)] is due to a group of magnetic reflections $(1-30)^-$, $(130)^-$, $(1-31)^-$, and $(131)^-$ that accidentally appear nearly at the same position as the nuclear reflection (110). This explains the variable-temperature dependence of the *J* reflection mentioned above. Note that we could not identify any changes in the symmetry of the material at this temperature. Therefore, it seems to be safe to use the symmetry group analysis based on the space-group *Cmmm*.

Among the eight rotational symmetry operations of the *Cmmm* space group, four of them leave the $q_I=(k_x,0,\frac{1}{2})$ propagation vector invariant. These are the identity 1, two-fold symmetry axis along the *a* axis 2 *x*, 0, 0, and two mirror planes—one in the *a*-*b* plane *m x*, *y*, 0, and the second in the *a*-*c* plane *m x*, 0, *z*. Consecutively, there are four one-dimensional irreducible representations (IRs) and four basic magnetic structure models that describe the possible mutual orientation of Er magnetic moments. These have been generated using the computer code MODY (Ref. 15) that is based on the symmetry group analysis[16] and are listed in Table II. All the moments are either oriented along or perpendicular to the *c* axis. Within the crystallographic unit cell, moments can be coupled either ferromagnetically or antiferromagnetically for $q_I=(k_x,0,\frac{1}{2})$ with $k_x\approx 0.16$ or only antiferromagnetically for $k_x\approx 0.84$. Note that the only difference between the two possible propagation vector models is the fact that magnetic moments on the Er_3 and the Er_4 positions are reversed. This might be, however, equivalently achieved by introducing a phase shift between Er_1 and Er_2 moments on one side, and Er_3 and Er_4 moments on the other that is close to π. After fitting the experimental data to all models, it appeared quite clear that the best agreement is found for a model following from IR Γ_1, belonging to $q_I=(0.8409(1),0,\frac{1}{2})$ with a small phase shift between moments at Er_1 and Er_2, and those at Er_3 and Er_4. Actually, the small value of the phase shift motivated us to use the propagation vector with $k_x\approx 0.84$ from the second Brillouin zone rather than from the first zone with $k_x\approx 0.16$. This holds also for all the incommensurate propagation vectors mentioned below.

The IR Γ_1 allows, in principle, both the *a*-axis and the *b*-axis components. However, only the *b*-axis component seems to be the significant one. The best fit of this model to the experimental data, taken at 3.07 K, is shown in Fig. 5(a). The inclusion of the *a*-axis component that is in principle allowed leads to a very marginal (if at all) improvement of the fit. One concludes that the *a*-axis moment component is less than 0.3 μ_B. The corresponding magnetic structure is schematically shown in Fig. 6(a).

TABLE II. Transformation rules for possible magnetic structure models belonging to different irreducible representations Γ that are in accord with the position 4*j* site of the *Cmmm* space group and relevant magnetic propagation vector q_i of the *i*th magnetic state, as derived by the symmetry group analysis. Sequence "+−−+" for $M(x_1x_2x_3x_4)$ denotes that the *x* component at the Er_1 site is coupled parallel to the *x* component at the Er_4 site and antiparallel to those at Er_2 and Er_3. Zero denotes that no such component is allowed.

		Γ_1	Γ_2	Γ_3	Γ_4	Γ_5	Γ_6	Γ_7	Γ_8
MS-I	$M(x_1x_2x_3x_4)$	+−−+	0000	0000	++−−				
$q_I=(0.8409(1),0,\frac{1}{2})$	$M(y_1y_2y_3y_4)$	++−−	0000	0000	+−−+	*x*	*x*	*x*	*x*
$T=3.07$ K	$M(z_1z_2z_3z_4)$	0000	++−−	+−−+	0000				
MS-II	$M(x_1x_2x_3x_4)$	+−−+	0000	0000	++−−				
$q_{II}=(0.5973(1),0,\frac{1}{2})$	$M(y_1y_2y_3y_4)$	++−−	0000	0000	+−−+	*x*	*x*	*x*	*x*
$T=2.37$ K	$M(z_1z_2z_3z_4)$	0000	++−−	+−−+	0000				
MS-III	$M(x_1x_2x_3x_4)$	+−−+	0000	0000	++−−				
$q_{III}=(0.5330(3),0,\frac{1}{2})$	$M(y_1y_2y_3y_4)$	++−−	0000	0000	+−−+	*x*	*x*	*x*	*x*
$T=1.97$ K	$M(z_1z_2z_3z_4)$	0000	++−−	+−−+	0000				
MS-IV	$M(x_1x_2x_3x_4)$	++−+	0000	0000	+−−−				
$q_{IV\text{-}1}=(\frac{1}{2},\frac{1}{2},\frac{1}{2})$	$M(y_1y_2y_3y_4)$	++−+	0000	0000	+−−−	*x*	*x*	*x*	*x*
	$M(z_1z_2z_3z_4)$	0000	+−−−	++−+	0000				
MS-IV	$M(x_1x_2x_3x_4)$	+−+−	0000		0000	0000	++++	0000	
$q_{IV\text{-}2}=(0,0,\frac{1}{2})$	$M(y_1y_2y_3y_4)$	0000	0000	*x*	++++	0000	0000	+−+−	*x*
	$M(z_1z_2z_3z_4)$	0000	++++		0000	+−+−	0000	0000	

D. Ground-state MS-IV phase in the low-temperature limit

Characteristic for the phase MS-IV stable below $T_{m3}=1.8$ K is the existence of reflections *A*, *D*, *F*, and *J* (that increase with lowering the temperature), and the absence of reflections belonging to the incommensurate magnetic phase MS-I. Reflections *E* and *H* still exist in this phase but decrease strongly as the temperature is reduced. Let us initially suppose that these latter reflections do not play a significant role. Using a trial and error approach, we could index all the remaining magnetic reflections with two propagation vectors, namely with $q_{IV\text{-}1}=(\frac{1}{2},\frac{1}{2},\frac{1}{2})$ and $q_{IV\text{-}2}=(0,0,\frac{1}{2})$. Possible magnetic structure models have been derived as for all of the other magnetic phases with the help of symmetry analysis and code MODY.[15,16] Also for this phase we have not observed any deviations from the original paramagnetic crystal structure symmetry, suggesting that there are no distortions also for the states between MS-I and MS-IV.

The existence of the $q_{IV\text{-}1}=(\frac{1}{2},\frac{1}{2},\frac{1}{2})$ propagation vector that contains half-indices naturally leads to a magnetic unit cell that has the lattice parameters doubled with respect to the crystallographic cell along all the three principal directions. The existence of the second propagation vector $q_{IV\text{-}2}=(0,0,\frac{1}{2})$ requires the doubling along the *c* axis only. One can therefore construct a magnetic unit cell that would contain 32 Er magnetic moments. Obviously, it would be tedious to perform the symmetry group analysis for such a large magnetic unit cell and to ascertain which model agrees at best with data. Therefore, we have fit our data to the model, having doubled lattice parameters constructed by using the symmetry analysis for the two propagation vectors individually.

At first sight one can exclude models Γ_2 and Γ_5 (see Table II) belonging to $q_{IV\text{-}2}$ that allow only the *c*-axis component because of the existence of the $(0\ 0\ \frac{1}{2})$ reflection. After fitting the data to all remaining possible magnetic structure models that have been constructed by combining the models belonging to $q_{IV\text{-}1}$ on one hand and to $q_{IV\text{-}2}$ on the other, it appeared that the best agreement is obtained for a model derived from IR Γ_4 belonging to $q_{IV\text{-}1}=(\frac{1}{2},\frac{1}{2},\frac{1}{2})$, combined with a model following from IR Γ_4, or Γ_6 belonging to $q_{IV\text{-}2}=(0,0,\frac{1}{2})$. The former representation allows for both the *a*-axis and the *b*-axis components simultaneously, the latter for the *a*-axis or the *b*-axis component only. All other models cannot correctly account for the observed intensities. The first question is whether there are both *a*-axis and *b*-axis components present for the Γ_4 part belonging to $q_{IV\text{-}1}=(\frac{1}{2},\frac{1}{2},\frac{1}{2})$. With the *a*-axis component set as a free parameter during the fitting procedure, one obtains little fit improvement and the *a*-axis component of less than 0.5 μ_B. The existence of such a component would lead, in combination with the Γ_6 model belonging to $q_{IV\text{-}2}=(0,0,\frac{1}{2})$, to nonequal Er moments and this is unlikely in the ground state. For the same reason one should also discard the model following from Γ_4 belonging to $q_{IV\text{-}2}$ that lead to strongly unequal *b*-axis moment components (and nonequal total Er moments). It is observed that the $(0\ 0\ \frac{1}{2})$ reflection increases with lowering the temperature, which would suggest that the Er moments become more and more unequal. This is contrary to the general expectation that magnetic structures tend to be buildup from equal-size moments at low temperatures. If one compares the best fits to [apart from Γ_4 belonging to $q_{IV\text{-}1}=(\frac{1}{2},\frac{1}{2},\frac{1}{2})$] IR Γ_6 and IR Γ_4, both belonging to $q_{IV\text{-}2}=(0,0,\frac{1}{2})$, one arrives to nearly identical agreements. While there is very little difference regarding low-intensity reflections [see the star denoted reflection around 30° in Fig. 5(d)], the resulting MS-IV magnetic structures are very different [schematically shown in Figs. 6(d) and 6(e)]. One is noncollinear, having equal-size Er moments

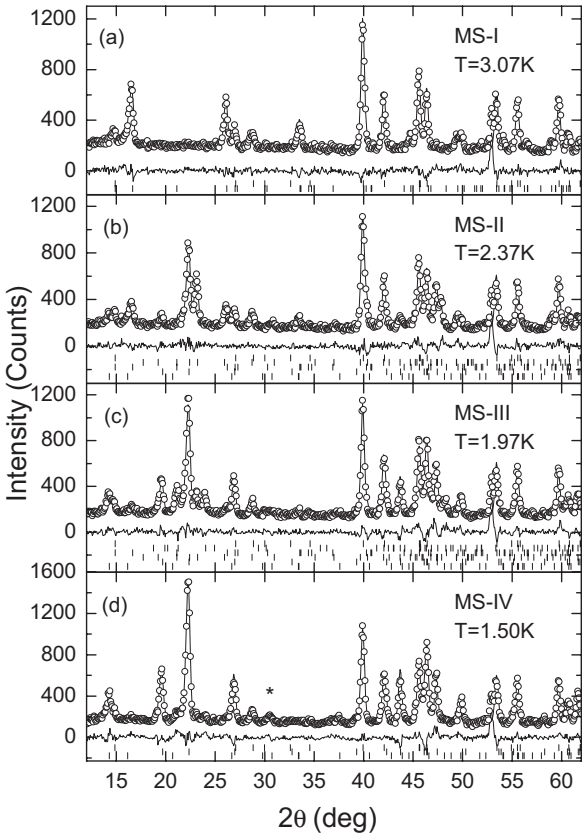

FIG. 5. The low-angle portion of the diffraction data (circles) of Er_2Ni_2Pb taken in the magnetic state at (a) 3.07, (b) 2.37, (c) 1.97, and (d) 1.50 K together with best fits (the full line through points) and the difference between them (line at the bottom of each panel). The positions of the magnetic and the crystal structure Bragg reflection positions are tick marked at the bottom. In panel (d) the fit model was derived from a combination of Γ_4 (belonging to $q_{\text{IV-1}}$) and Γ_4 ($q_{\text{IV-2}}$) irreducible representations. The fit model derived from Γ_4 ($q_{\text{IV-1}}$) and Γ_6 ($q_{\text{IV-2}}$) IRs differs only in a slightly worse description of reflections around the scattering angle of 30° (marked by a star). The schematic representations of the individual magnetic structures are shown in Fig. 6. For numerical results, see Table III.

in the *a*-*b* plane [Fig. 6(d)]; the other, slightly preferred, is collinear with unequal Er moments directed along the *b* axis [Fig. 6(e)]. All the numerical results are listed in Table III. It should be noted that similar collinear nonequal magnetic-moment arrangement has been observed also in the ground-state magnetic phase of the isostructural Ho_2Ni_2Pb.[10]

E. MS-II state between the $T_{m1}=3.0$ K and $T_{m2}=2.3$ K

Characteristic for the phase stable between $T_N=3.5$ K and $T_{m1}=3.0$ K is existence of reflections *C* and *I* that are present already in the MS-I phase (see Sec. III C). Another characteristic is the appearance of new reflections *F* and *G*, which are, however, not indexable with the propagation vector mentioned above but require a new one, namely $q_{\text{II}}=(k_x,0,\frac{1}{2})$ with $k_x\approx 0.59$. With such a propagation vector one can identify the *F* reflection as being a group of $(0-11)^-$, $(010)^+$, $(010)^-$, and $(011)^-$ magnetic Bragg reflections, and the *G* reflection as being composed from $(1-21)^-$, $(120)^-$, $(1-20)^-$, and $(121)^-$ magnetic Bragg reflections. The symmetry analysis leads to results (the same ones as for the phase MS-I) that are summarized in Table II. The difference with respect to the MS-I magnetic state is, however, the fact that we deal with the coexistence of more than one propagation vectors. Thus, in addition to the reflections described by propagation vector $q_{\text{II}}=(k_x,0,\frac{1}{2})$ with $k_x\approx 0.59$, we must also consider MS-I reflections that are described by vector $q_{\text{I}}=(k_x,0,\frac{1}{2})$ with $k_x\approx 0.84$. While the latter set of reflections are explainable with the very same coupling between the Er moments as before, the arrangement for the former part has to be extracted by the trial and error method.

After fitting the experimental data to all models, it appeared quite clear that the best description of the q_{II} reflections is found for a model following from IR Γ_4 with a nonzero phase shift between moments at the Er_1 and Er_2 sites relative to the Er_3 and Er_4 sites. Again, only the *b*-axis component seems to be significant with the *a*-axis moment component smaller than 0.5 μ_B.

Due to extensive temperature overlap of reflections (see Figs. 3 and 4) belonging to another phase (namely, the MS-IV that was described in the Sec. III D) in this temperature range, we have to include all of them in the refinement. The new reflections of the phase MS-III that will be described in the next section could be neglected. The best fit of the model that comprises four components described by four propagation vectors (q_{II}, q_{I}, $q_{\text{IV-1}}$, and $q_{\text{IV-2}}$) to the experimental data taken at 2.37 K is shown in Fig. 5(b). The numerical results are listed in Table III. The magnetic structure resulting from the q_{II} propagation vector only is shown in Fig. 6(b).

As is generally known on the basis of neutron diffraction results, one cannot conclude whether a certain magnetic structure extends over the whole volume of the sample and needs, for its full description, several propagation vectors or whether several, spatially separated regions, each having smaller number of propagation vectors, exist. This follows from the fact that the measured intensity of a certain reflection (if incommensurate corresponding to a certain Fourier component) is proportional to the diffraction volume and to the square of the magnetic moment.

By considering the former possibility, one realizes that the obvious problem is the magnitude of the magnetic moment. Such is apparent when one considers that the first two contributions described by q_{II} and q_{I} have periodicities that are both incommensurate. This means that if the magnetic structure would be in an entire sample volume and described by both propagation vectors simultaneously, there would exist Er moments with magnitude of $6.93(10)+4.41(10)=11.34(20)\mu_B$. This is clearly much higher than the maximum possible saturated moment for Er^{3+} ion that amounts to 9 μ_B. The inclusion of the two remaining components belonging to $q_{\text{IV-1}}$ and $q_{\text{IV-2}}$ makes the situation even worse. Thus, it seems to be safe to conclude that in Er_2Ni_2Pb several, spatially (volume) separated magnetic structures coexist at 2.37 K. It is difficult to conclude what volume fraction each phase occupies if one does not know the magnetic-moment magnitudes involved at the particular temperature. This problem will be tackled later.

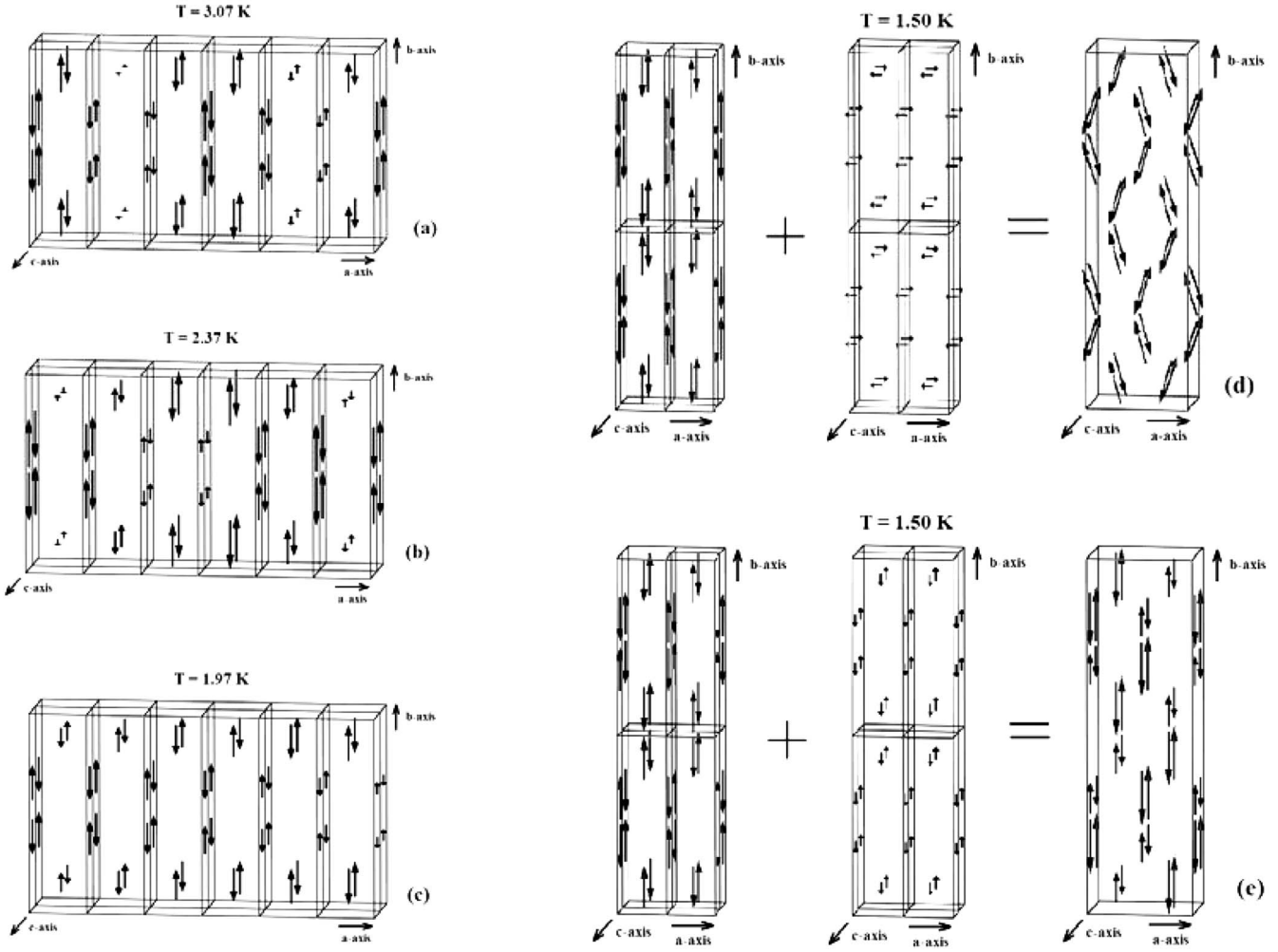

FIG. 6. The schematic of the refined magnetic structures derived from irreducible representations belonging to individual propagation vectors (a) $\Gamma_1(q_{\mathrm{I}})$, (b) $\Gamma_4(q_{\mathrm{II}})$, (c) $\Gamma_4(q_{\mathrm{III}})$, (d) $\Gamma_4(q_{\mathrm{IV\text{-}1}})$ combined with $\Gamma_6(q_{\mathrm{IV\text{-}2}})$, and (e) $\Gamma_4(q_{\mathrm{IV\text{-}1}})$ combined with $\Gamma_4(q_{\mathrm{IV\text{-}2}})$. In the (a)–(c) panels, twelve crystallographic unit cells ($6a\times1b\times2c$) and only magnetic moments are shown. In the panels (d) and (e), eight crystallographic ($2a\times2b\times2c$) unit cells and only magnetic moments are shown.

F. MS-III state between the $T_{m2}=2.3$ K and $T_{m3}=1.8$ K

Characteristic for this state is the existence of all the reflections mentioned above, and further reflections F and H that appear at $T_{m2}=2.2$ K, exhibit maximum at 2.0 K, and fade away with further lowering of the temperature. At 1.5 K, the lowest temperature of the experiment, F and H still do exist (see Figs. 3 and 4) but were neglected for simplicity in Sec. III D. Below 2.0 K their intensity falls steeply, followed below 1.8 K by a much slower further decrease. At 1.5 K their intensities reach about 20% of their maximal intensity. That is why we have selected the temperature of 1.8 K as the magnetic phase transition T_{m3}. Both of them $(F+H)$ can be indexed with a new propagation vector $q_{\mathrm{III}}=(k_x,0,\frac{1}{2})$ with $k_x\approx0.54$. The F reflection is identified as being composed from $(0-11)^-$, $(010)^+$, $(010)^-$, and $(011)^-$ reflections, and the H as being a conglomerate of $(1-20)^-$, $(120)^-$, $(1-21)^-$, and $(121)^-$ magnetic Bragg reflections.

The symmetry analysis for this phase leads to results identical to those obtained for phase MS-II. For completeness they are summarized in Table II. During the refinement, we cannot ignore, similar to the phase MS-II, the coexistence of different propagation vectors. In fact, we have to include all propagation vectors mentioned so far: (i) $q_{\mathrm{III}}=(k_x,0,\frac{1}{2})$ with $k_x\approx0.54$ that describes the new reflections F and H, (ii) $q_{\mathrm{I}}=(k_x,0,\frac{1}{2})$ with $k_x\approx0.84$ to account for the MS-I reflections, (iii) $q_{\mathrm{II}}=(k_x,0,\frac{1}{2})$ with $k_x\approx0.59$ that account for the MS-II reflections, and finally (iv) both $q_{\mathrm{IV\text{-}1}}=(\frac{1}{2},\frac{1}{2},\frac{1}{2})$ and $q_{\mathrm{IV\text{-}2}}=(0,0,\frac{1}{2})$ of the ground-state state MS-IV. While for the latter four sets of reflections, the relevant couplings between the Er moments are known; the arrangement for the former part (q_{III}) has to be found by fitting all the possible models and selecting the one that gives the best agreement.

As for MS-III it appeared quite clear that the best description is found for a model following from IR Γ_4. Similar to the MS-II phase, there is a significant phase shift between moments at the Er_1 and Er_2 sites, and those at Er_3 and Er_4. It seems that also here, only the b axis is a significant component of the MS-III magnetic structure with the a-axis moment component smaller than 0.7 μ_B. The best fit of the model using all five propagation vectors (q_{III}, q_{I}, q_{II}, $q_{\mathrm{IV\text{-}1}}$,

TABLE III. Structural and magnetic parameters of Er_2Ni_2Pb determined at 3.07 (MS-I state), 2.37 (MS-II state), 1.97 (MS-III state) and 1.50 K (MS-IV state) using powder neutron diffraction. For the MS-IV state two results are given: combination of $\Gamma_4(q_{IV\text{-}1})$ and $\Gamma_6(q_{IV\text{-}2})$, leading to noncollinear magnetic structure, and combination $\Gamma_4(q_{IV\text{-}1})$ and $\Gamma_4(q_{IV\text{-}2})$, leading to collinear magnetic structure (bottom).

MS-I, $T=3.07$ K		Er moment components	
IR: propagation vector	μ_x (μ_B)	μ_y (μ_B)	μ_z (μ_B)
Γ_1: $q_I=(0.8409(1),0,\frac{1}{2})$	<0.3	6.08 (9)	0
Agreement factors:	$R_p=6.58\%$	$R_B=7.73\%$	$R_M=9.42\%$
MS-II, $T=2.37$ K		Er moment components	
IR: propagation vector	μ_x (μ_B)	μ_y (μ_B)	μ_z (μ_B)
Γ_1: $q_I=(0.8426(1),0,\frac{1}{2})$	<0.3	4.41 (10)	0
Γ_4: $q_{II}=(0.5974(1),0,\frac{1}{2})$	<0.5	6.93 (10)	0
Γ_4: $q_{IV\text{-}1}=(\frac{1}{2},\frac{1}{2},\frac{1}{2})$	<0.5	2.57 (9)	0
Γ_4: $q_{IV\text{-}2}=(0,0,\frac{1}{2})$	<0.5	1.03 (9)	0
Agreement factors:	$R_p=6.92\%$	$R_B=7.20\%$	$R_M=11.4\%$
MS-III, $T=1.97$ K		Er moment components	
IR: propagation vector	μ_x (μ_B)	μ_y (μ_B)	μ_z (μ_B)
Γ_1: $q_I=(0.0.8438(6),0,\frac{1}{2})$	<0.3	2.64 (14)	0
Γ_4: $q_{II}=(0.5977(3),0,\frac{1}{2})$	<0.5	4.19 (14)	0
Γ_4: $q_{III}=(0.5330(3),0,\frac{1}{2})$	<0.7	4.89 (11)	0
Γ_4: $q_{IV\text{-}1}=(\frac{1}{2},\frac{1}{2},\frac{1}{2})$	<0.5	5.29 (7)	0
Γ_4: $q_{IV\text{-}2}=(0,0,\frac{1}{2})$	<0.5	1.57 (6)	0
Agreement factors:	$R_p=7.32\%$	$R_B=6.97\%$	$R_M=9.90\%$
MS-IV, $T=1.50$ K		Er moment components	
IR: propagation vector	μ_x (μ_B)	μ_y (μ_B)	μ_z (μ_B)
Γ_4: $q_{IV\text{-}1}=(\frac{1}{2},\frac{1}{2},\frac{1}{2})$	<0.5	6.78 (11)	0
Γ_6: $q_{IV\text{-}2}=(0,0,\frac{1}{2})$	1.92 (6)	0	0
Agreement factors:	$R_p=8.49\%$	$R_B=8.87\%$	$R_M=11.5\%$
MS-IV, $T=1.50$ K		Er moment components	
IR: propagation vector	μ_x (μ_B)	μ_y (μ_B)	μ_z (μ_B)
Γ_4: $q_{IV\text{-}1}=(\frac{1}{2},\frac{1}{2},\frac{1}{2})$	<0.5	6.73 (4)	0
Γ_4: $q_{IV\text{-}2}=(0,0,\frac{1}{2})$	0	1.90 (3)	0
Agreement factors:	$R_p=8.05\%$	$R_B=8.17\%$	$R_M=10.3\%$

and $q_{IV\text{-}2}$) to the experimental data taken at 1.97 K is shown in Fig. 5(c). The numerical results are listed in Table III. The magnetic structure resulting from the q_{III} propagation vector only is shown in Fig. 6(c).

Also for the MS-II state, it is safe to conclude that it is not defined by all the propagation vectors simultaneously (if one sums all the components, one arrives to Er moment magnitude of nearly 19 μ_B), but that several, spatially separated magnetic structures coexist at 1.97 K.

IV. DISCUSSION

Refinement of the diffractogram taken above the magnetic phase transition in the paramagnetic state showed clearly that the Er_2Ni_2Pb forms as suggested in the literature[2] with the orthorhombic crystal structure (*Cmmm* space group). The extra reflections seen at 4.5 K were identified as being due to the sample environment. The crystal structure of Er_2Ni_2Pb has lattice constants of very different length and consequently we had to introduce the preferential orientation already when refining the paramagnetic crystal structure pattern. The positional parameters are in very good agreement with literature values.[2]

The literature sources for Er_2Ni_2Pb suggested either a magnetic phase-transition temperature of $T_{N1}=3.4$ K into a complex, most probably antiferromagnetic state followed by two order-order magnetic phase transitions at $T_{N2}=3.2$ K

and $T_{N3}=2.0$ K,[4,6] or a magnetic phase transition $T_C=6.0$ K toward a ferromagnetic state with a subsequent antiferromagnetic transition at 3.5 K.[3]

Our neutron diffraction results are clearly in accord with the former suggestion. The appearance of new Bragg reflections below $T_N=3.5$ K that are indexable with an incommensurate propagation vector $q_I=(0.84,0,\frac{1}{2})$ rejects the suggestion for ferromagnetic order in Er_2Ni_2Pb. The fact that below $T_{m1}=3.0$ K, $T_{m2}=2.3$ K, and finally $T_{m3}=1.8$ K, new Bragg reflections indexable with $q_{II}=(0.59,0,\frac{1}{2})$, $q_{III}=(0.54,0,\frac{1}{2})$, $q_{IV\text{-}1}=(\frac{1}{2},\frac{1}{2},\frac{1}{2})$, and $q_{IV\text{-}2}=(0,0,\frac{1}{2})$ all show how complex the antiferromagnetic order in Er_2Ni_2Pb is. Although the possible magnetic structures between $T_N=3.5$ K and $T_{m3}=1.8$ K are incommensurate, both propagation vectors for the magnetic structure at the low-temperature limit are strictly antiferromagnetic.

In the entire neutron data analysis, we have supposed that the crystal lattice symmetry is preserved at all the temperatures below T_N. With such an assumption and the knowledge of the relevant propagation vector, one can use the symmetry group analysis that yields possible magnetic structures. This approach can be used, however, only if the magnetic phase transition is of the second order and no distortion takes place. Although the temperature dependence of specific heat, as shown in Fig. 4. of Ref. 4, shows a relatively sharp anomaly around $T_{N2}=3.2$ K that could indicate a first-order transition, we could not discern either any distortion in the crystal structure of the material or a significant hysteresis around this temperature. Moreover, the absence of crystal structure modifications in the closely related Dy_2Ni_2Pb, which was checked by x-ray diffraction at low temperatures,[17] gives us confidence that such an approach is justified.

The arrangement of Er magnetic moments for each of the identified propagation vectors has been deduced by a trial and error procedure, in which all the magnetic models suggested by the symmetry analysis were fitted to the relevant experimental data. While the magnetic structure of the state MS-I was identified as being a "stand-alone" ordinary sine-wave transverse modulated with the Er magnetic-moment magnitude of $6.08(9)\mu_B$, the situation for the remaining phases is more complex because of the simultaneous existence of several propagation vectors.

As mentioned already in Sec. III E, it is, in principle, impossible without knowledge of additional magnetic information to decide whether a certain magnetic phase consists of several spatially separated magnetic structures (each defined by another, possibly single, propagation vector, the so-called single-k domains) or whether it is defined by more propagation vectors at the same time (the so-called multiple-k structure). On the basis of results given in Secs. III E and III F, it is clear that the magnetic states between $T_{m1}=3.0$ K and $T_{m3}=1.8$ K consist from several spatially separated single-k magnetic phases. It is hard to deduce their volume fraction if one does not know the relevant magnetic-moment magnitudes. However, one can at least estimate the fractions by supposing that the moment magnitudes are, in all magnetic structures, equal and the whole sample volume is magnetically ordered. With such an assumption, one arrives to the temperature dependences of volume fractions belonging to magnetic phases described by q_I, q_{II}, q_{III}, $q_{IV\text{-}1}$, and $q_{IV\text{-}2}$ propagation vectors, respectively, which are shown in Fig. 7. The corresponding magnetic moment is shown in Fig. 7 as stars. Note that we have treated the two propagation vectors, $q_{IV\text{-}1}$ and $q_{IV\text{-}1}$, as describing spatially disjunctive magnetic phases. The temperature dependence of the magnetic-moment magnitude seems to be in a good agreement with the expected temperature dependence and is nearly identical to that observed for the related Ho_2Ni_2Pb compound (see Fig. 16 in Ref. 10), with the exception of the temperatures below about 2 K (in the MS-IV region). In the analysis of the phase at 1.5 K, we have assumed that all the magnetic Bragg reflections appearing below T_{m3} belong to the same magnetic structure, i.e., the magnetic structure occupies the whole volume of the sample and it is defined by both magnetic propagation vectors simultaneously. In Sec. III D it was shown that the model, having collinear arrangement of nonequal magnetic moments, gives slightly better agreement with experimental data. However, such magnetic structure is rather unusual. Although the maximum moment magnitude of $6.73(4)+1.90(3)=8.63(7)\mu_B/\mathrm{Er}$, is again close to the expected moment, such a superposition appears to be unphysical. We expect from entropy arguments[18] that in the low-temperature limit, the magnetic structure tend to be built up from equal magnetic moments. It is, however, experimentally proven (see Figs. 3 and 4) that the reflection A [identified as being $(0\ 0\ \frac{1}{2})$] increases in intensity upon lowering the temperature. Thereby it introduces larger and larger differences in the Er magnetic moments if one considers the magnetic structure to be determined by both propagation vectors simultaneously. It is therefore natural to suppose that we deal, also in this magnetic state, with spatially separated magnetic phases. The analysis of the 1.5 K diffractogram, taking into account the existence of the weak E and H reflections (remaining from the MS-III), and, supposing that all the relevant phases are separated and are built from magnetic moments of the same size, leads to the value of $7.4(1)\mu_B/\mathrm{Er}$, which is not that different from the saturated magnetization value of 8 μ_B/Er when measured along the b axis.[4] Such a moment is noticeably reduced with respect to the free Er^{3+} ion value of $9\mu B$ and this might be a signature of crystal

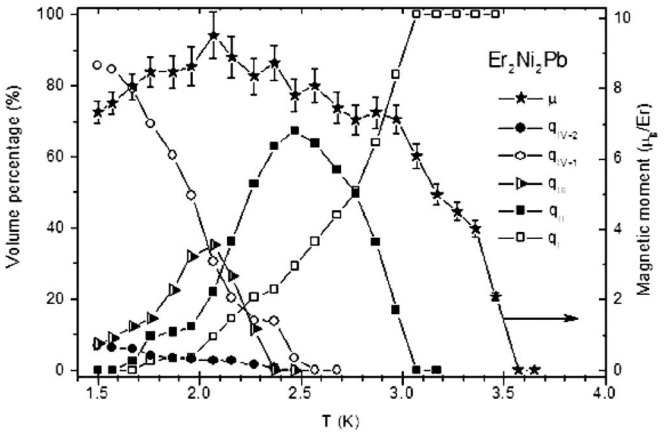

FIG. 7. The temperature dependence of the volume fractions of different magnetic phases and of the magnetic-moment magnitude, which was derived with the assumptions that it is identical, in all the coexisting magnetic phases.

electric-field (CEF) effects. We believe, however, that CEF effects cannot explain the discrepancy alone because much larger magnetic moments are obtained at higher temperatures. It would be highly anomalous that the moment would decrease upon lowering the temperature. Thus, it seems that, in contrast to the magnetic states at elevated temperatures, the ground-state magnetic structure is not completely solved and warrants further study. A single crystal and even lower temperatures would be highly desirable in order to clarify whether the magnetic phase described by propagation vector $q_{\text{IV-2}}$ prevails in the low-temperature limit or whether the two phases ($q_{\text{IV-1}}+q_{\text{IV-2}}$) coexist down to the lowest temperatures. Of a great importance would be muon spin resonance or NMR experiments that should be able to answer unambiguously the question regarding the magnetic homogeneity of the sample.

Let us now consider the reasons for the coexistence of magnetic phases in Er_2Ni_2Pb. The Er atoms form two nearly isosceles triangular chains running along the *a* axis that are separated by the *c* axis parameter $c=\Delta_4=3.61$ Å (which is also the nearest-neighbor Er distance). The shortest distance between the Er atoms within the chains is $\Delta_2=3.66$ Å (next-nearest-neighbor separation). One realizes that the two chains within the *a*-*b* plane form in fact a two-dimensional (2D) network. Every second, Er atoms are separated by $\Delta_1=3.88$ Å in the positive and the negative direction along the *b* axis, which represents the next-next-nearest-neighbor distance. Finally, the next separation is found along the a axis and amounts to $\Delta_3=4.00$ Å. We now argue that such an arrangement can lead to magnetic frustration due to competing AF and F interactions along the three links connecting Er atoms in the *a*-*b* plane. Competing interaction in the presence of magnetocrystalline anisotropy are a well-known origin for unequal or reduced moments and can lead to very complicated noncollinear magnetic structures[18] especially in rare-earth compounds.[19] While the interaction along the shortest *c*-axis link remains antiferromagnetic for all the magnetic structures that causes a doubling of the unit cell in this direction, the competition of AF and F interactions along the *a* and *b* axes leads to a variety of different magnetic structures that can coexist in certain temperature region. For instance, in the q_{I} magnetic structure the interaction along the Δ_1 link is ferromagnetic and along Δ_2 mostly antiferromagnetic. The type of the interaction is, however, just reversed for the q_{II} and q_{III} magnetic structures. If one neglects the fact that the chains are formed in a zigzag manner, this phase can be represented by a sequence "++−−" along the *a* axis. This arrangement is known to be very stable. For the other low-temperature structure, $q_{\text{IV-2}}$, both interactions are ferromagnetic independently, of which the models (Γ_4 or Γ_6) are considered.

V. CONCLUSION

We have presented the results of a comprehensive powder neutron diffraction study in zero field performed on single phase Er_2Ni_2Pb. The paramagnetic powder-diffraction pattern can be fully explained within the crystal structure suggested in the literature.[2] All the new Bragg reflections that appear below $T_N=3.5$ K could be indexed with several different propagation vectors that are partly overlapping in temperature. Based upon fitting the neutron diffraction patterns to models allowed by symmetry, the Er_2Ni_2Pb compound has been found to exhibit antiferromagnetic ordering at all temperatures. It appears that the most plausible explanation for the simultaneous appearance of several propagation vectors is spatially separated magnetic phases. Each phase is described by a single propagation vector that appears due to competing magnetic interactions and anisotropy. With the assumption that all of the phases are build up from magnetic moments of equal maximal magnitude (i.e., defining the height of sine-wave modulated Er moments propagating along the *a* axis), we arrive at a fairly reasonable model for all the phases above 1.8 K. Yet a certain discrepancy in the moment magnitudes exists for the magnetic state found at the lowest temperature of the experiment at 1.5 K. Namely, the moments are found to be smaller than those at more elevated temperatures and reduced with respect to the Er^{3+} value. This finding is partially attributed to crystal-field effects but some ambiguity regarding the details of the ground-state magnetic structure still exists. We suggest that single-crystal neutron diffraction, muon spin resonance, or NMR experiments should resolve the problem.

ACKNOWLEDGMENTS

This work was supported by the Dutch NWO and FOM Foundations, CONACyT (Mexico) through Grants No. G-25851 and No. 39643-F, and by the European Commission Contract No. HPRICT-2001-00138 access to research infrastructures. We wish to acknowledge the competent assistance of R. W. A. Hendrikx and T. J. Gortenmulder in the sample preparation and analysis. K.P. would like to express his thanks to Th. Wiechmann from the Klinikum Ernst von Bergmann gGmbH Potsdam and the whole team of the E4 station for their hospitality and perfect medical care during his stay.

[1] *Handbook of Magnetic Materials*, edited by K. H. J. Buschow (Elsevier, Amsterdam/North-Holland, Amsterdam, 1980–2001), Vols. 1-13.

[2] L. D. Gulay, Y. M. Kalychak, and M. Wolcyrz, J. Alloys Compd. **311**, 228 (2000).

[3] L. D. Gulay and K. Hiebl, J. Alloys Compd. **351**, 35 (2003).

[4] A. D. Chinchure, E. Muñoz Sandoval, and J. A. Mydosh, Phys. Rev. B **66**, 020409(R) (2002).

[5] K. Prokeš, E. M. Sandoval, A. D. Chinchure, and J. A. Mydosh, Phys. Rev. B **68**, 134427 (2003).

[6] A. D. Chinchure, E. Muñoz-Sandoval, and J. A. Mydosh, Phys. Rev. B **64**, 020404(R) (2001).

[7] E. Muñoz-Sandoval, A. D. Chinchure, R. W. A. Hendrikx, and J. A. Mydosh, Europhys. Lett. **56**, 302 (2001).
[8] A. D. Chinchure, E. Muñoz-Sandoval, T. J. Gortenmulder, R. W. A. Hendrikx, and J. A. Mydosh, J. Alloys Compd. **359**, 5 (2003).
[9] V. Goruganti,Y. Li, J. H. Ross, Jr., K. D. D. Rathnayaka, and Y. Öner, J. Appl. Phys. **99**, 08P303 (2006).
[10] K. Prokeš, E. Muñoz-Sandoval, A. D. Chinchure, and J. A. Mydosh, Eur. Phys. J. B **43**, 163 (2005).
[11] J. L. Daams, P. Villars, and J. H. N. van Vucht, *Atlas of Crystal Structure Types for Intermetallic Phases* (ASM, Metals Park, OH, 1991).
[12] H. M. Rietveld, J. Appl. Crystallogr. **2**, 65 (1969).
[13] T. Roisnel and J. Rodríguez-Carvajal, Mater. Sci. Forum **378**, 118 (2001).
[14] V. F. Sears, Neutron News **3**, 26 (1992).
[15] W. Sikora, F. Bialas, L. Pytlik, and J. Malinowski, J. Appl. Crystallogr. **37**, 1015 (2004).
[16] E. F. Bertaut, Acta Crystallogr., Sect. A: Cryst. Phys., Diffr., Theor. Gen. Crystallogr. **24**, 217 (1968).
[17] S. Daniš, K. Prokeš, E. Muñoz-Sandoval, A. D. Chinchure, and J. A. Mydosh (unpublished).
[18] J. Rossat-Mignod, in *Neutron Physics*, edited by K. Skold and D. L. Price (Academic, New York, 1987), Vol. 23C, p. 69.
[19] W. Suski, in *Handbook on the Physics and Chemistry of Rare Earths*, edited by K. A. Gschneidner, Jr. and L. Eyring (Elsevier Science, Amsterdam, 1996), Vol. 22, Chap. 146, p. 143.